Supplement of Atmos. Chem. Phys., 18, 15017–15046, 2018
https://doi.org/10.5194/acp-18-15017-2018-supplement

Atmospheric Chemistry and Physics
Open Access
EGU

Supplement of

Adjoint inversion of Chinese non-methane volatile organic compound emissions using space-based observations of formaldehyde and glyoxal

Hansen Cao et al.

Correspondence to: Tzung-May Fu (tmfu@pku.edu.cn)

Table S1 Ultimate yields of formaldehyde and glyoxal from the oxidation of NMVOC precursors by OH in our model under high-NO_x and low-NO_x conditions

NMVOCs	Formaldehyde (molecules per C)		Glyoxal (molecules per C)	
	High-NO_x [a]	Low-NO_x [b]	High-NO_x [a]	Low-NO_x [b]
Ethene	0.995	0.366	0.0665	0.067
Glycolaldehyde	0.366	0.366	0.067	0.067
Isoprene	0.436	0.38	0.0255	0.073
2-methyl-3-bute-nol (MBO)	0.092	0.092	0.0168	0.0168
Benzene	0.001	0.001	0.0555	0.0555
Toluene	0.198	0.18	0.037	0.037
Xylenes	0.269	0.155	0.026	0.026
Monoterpenes (lumped)	0.006	0.006	0.005 [c]	0.005 [c]
Ethyne	-	-	0.318	0.318
Methanol	1.0	1.0	-	-
Ethane	0.5	0.5	-	-
Acetaldehyde (lumped)	0.5	0.5	-	-
Propane	0.49	0.317	-	-
$\geq C_3$ alkenes (lumped)	0.657	0.333	-	-
Acetone	0.64	0.383	-	-
Hydroxyacetone	0.333	0.333	-	-
Methyglyoxal	0.333	0.333	-	-
$\geq C_4$ alkanes (lumped)	0.578	0.187	-	-
Methy ethyl ketone (lumped)	0.465	0.25	-	-

[a] Yields under high-NO_x conditions were calculated assuming that all RO_2 radicals from the oxidation of the NMVOC precursor reacted with NO.

[b] Yields under low-NO_x conditions were calculated assuming RO_2:HO_2 concentration ratio of 1:1.

[c] Glyoxal produced from the oxidation of monoterpenes by ozone

Table S2 Technical details for the GOME-2A and OMI formaldehyde and glyoxal observations used in this study

Technical details		GOME-2A		OMI	
		Formaldehyde	Glyoxal	Formaldehyde	Glyoxal
Product reference		De Smedt et al. (2012)	Lerot et al. (2010)	González Abad et al. (2015)	Chan Miller et al. (2014)
Platform		European MetOp-A satellite		NASA Aura satellite	
Operation time		October 2006 – present		July 2004 – present	
Overpass time		9:30 local time		13:30 local time	
Global coverage		Every 1.5 days before June 2013; every 3 days after June 2013		Every 1 day	
Spatial resolution		80 km × 40 km		13 km × 24 km	
Spectral window		240-790 nm		270-500 nm	
Spectral resolution		0.26-0.5 nm		0.42 nm and 0.63 nm	
Selected absorption band		328.5 - 346 nm	435 - 460 nm	328.5 - 356.5 nm	435 - 461 nm
Retrieval algorithm		Differential Optical Absorption Spectroscopy (DOAS) fitting		Direct fitting	
Cloud parameter data		FRESCO+ (Wang et al., 2008)		OMCLDO2 (Acarreta et al., 2004)	
Surface albedo data		Kleipool et al. (2008)		Kleipool et al. (2008)	
Air mass factor calculation	Radiative transfer model	LIDORT (Spurr, 2008)		VLIDORT (Spurr, 2006)	
	Tracer gas profiles	IMAGES model outputs (Stavrakou et al., 2009b)		GEOS-Chem model outputs (González Abad et al., 2015)	
Extinction by aerosols		Considered implicitly via cloud correction (Boersma et al., 2004)		Considered implicitly in the cloud retrieval (Acarreta et al., 2004)	
Discarded pixels		Pixels with cloud fraction >40% or zenith angles >60^{o} were discarded		Pixels with cloud fraction > 40% were discarded	Pixels flagged as impacted by random telegraph signals were discarded [a]

[a] Some pixels were flagged as impacted by random telegraph signals in the level 1-B product (Kleipool, 2005).

Table S3 Ground-based MAX-DOAS measurements of formaldehyde and glyoxal vertical column densities in China at GOME-2A and OMI overpass times

Reference	Location	Time of measurement		Vertical column densities	
				9-10 local time	13-14 local time
Formaldehyde [10^{16} molecules cm^{-2}]					
Vlemmix et al. (2015)	Xianghe, Hebei (39.75N, 116.96E)	2010-2016	JAN	0.51 ±0.17	0.82 ±0.17
			FEB	0.70 ±0.07	0.95 ±0.04
			MAR	0.89 ±0.12	1.12 ±0.17
			APR	1.04 ±0.11	1.21 ±0.16
			MAY	1.39 ±0.19	1.87 ±0.28
			JUN	1.86 ±0.25	2.41 ±0.24
			JUL	1.75 ±0.27	2.16 ±0.15
			AUG	1.67 ±0.20	2.18 ±0.22
			SEP	1.24 ±0.21	1.57 ±0.17
			OCT	1.17 ±0.15	1.49 ±0.14
			NOV	0.80 ±0.03	1.11 ±0.15
			DEC	0.61 ±0.13	0.89 ±0.07
Lee et al. (2015)	Beijing (39.59°N, 116.18°E)	August 16 to September 11, 2006		-	1.79
Wang et al. (2017)	Wuxi, Jiangsu (31.57°N,120.31°E)	2011 – 2014	JF	0.7 [a]	0.8 [a]
			MA	0.9 ±0.15 [a]	1.1 ±0.26 [a]
			MJ	1.5 ±0.12 [a]	1.9 ±0.15 [a]
			JA	1.7 ±0.10 [a]	2.2 ±0.26 [a]
			SO	1.2 ±0.12 [a]	1.7 ±0.12 [a]
			ND	0.8 ±0.30 [a]	1.4 ±0.32 [a]
Li et al. (2013)	Back Garden, Guangdong (23.50°N, 113.03°E)	July 2006		1.3 ±1.0 [b]	1.3 ±0.7 [b]
Glyoxal [10^{14} molecules cm^{-2}]					
Li et al. (2013)	Back Garden, Guangdong (23.50°N, 113.03°E)	July 2006		6.8 ±5.2 [c]	11.4 ±6.8 [c]

[a] From Figure 12 of Wang et al. (2017)

[b] From Figure 4 of Li et al. (2013)

[c] From Figure 5 of Li et al. (2013)

Table S4 Statistical comparisons of the *a priori* and *a posteriori* (from IE-1) simulated formaldehyde VCDs against the formaldehyde VCDs observed by GOME-2A over eastern China [a]

Month	Formaldehyde VCD comparisons (model against GOME-2A observations)					
	NMB [b]		R [b]		RMSE [b] ($\times 10^{15}$ molecules cm^{-2})	
	a priori	*a posteriori* IE-1	*a priori*	*a posteriori* IE-1	*a priori*	*a posteriori* IE-1
JAN	0.43	0.066	0.80	0.92	2.12	0.645
FEB	0.13	-0.036	0.80	0.92	1.59	0.947
MAR	-0.024	-0.064	0.94	0.97	1.29	1.10
APR	0.11	0.047	0.93	0.97	1.25	0.83
MAY	-0.099	0.044	0.87	0.97	1.50	1.21
JUN	-0.11	0.005	0.80	0.87	2.27	1.93
JUL	-0.064	0.042	0.81	0.87	1.87	1.71
AUG	0.014	0.074	0.85	0.87	1.31	1.46
SEP	0.017	0.051	0.83	0.87	1.25	1.15
OCT	0.13	0.04	0.90	0.95	1.31	0.809
NOV	0.45	0.13	0.74	0.94	2.28	1.00
DEC	0.67	0.17	0.51	0.85	3.27	1.19

[a] The eastern China domain is defined as the area within the red dashed box (20^oN-42^oN,103^oE-123^oE) in Figure 3 of the main text.

[b] NMB: normalized mean bias; R: Pearson correlation coefficient; RMSE: root mean square error

Table S5 Statistical comparisons of the *a priori* and *a posteriori* (from IE-3) simulated formaldehyde VCDs against the 1.7 times the formaldehyde VCDs observed by GOME-2A over eastern China [a]

Month	Formaldehyde VCDs (model against GOME-2A observations ×1.7)					
	NMB [b]		R [b]		RMSE [b] ($\times10^{15}$ molec cm^{-2})	
	a priori	*a posteriori* IE-3	*a priori*	*a posteriori* IE-3	*a priori*	*a posteriori* IE-3
JAN	0.092	-0.054	0.71	0.89	1.56	0.880
FEB	-0.20	-0.21	0.76	0.82	2.75	2.63
MAR	-0.32	-0.22	0.93	0.88	4.30	3.79
APR	-0.19	-0.18	0.92	0.94	2.96	2.78
MAY	-0.39	-0.15	0.85	0.92	5.12	2.51
JUN	-0.41	-0.15	0.78	0.93	7.64	3.84
JUL	-0.37	-0.19	0.80	0.92	6.79	3.62
AUG	-0.31	-0.17	0.85	0.90	4.69	2.77
SEP	-0.28	-0.11	0.82	0.93	3.64	1.73
OCT	-0.16	-0.12	0.89	0.92	2.46	1.98
NOV	0.12	-0.10	0.62	0.90	2.55	1.99
DEC	0.30	-0.048	0.38	0.82	3.14	1.80

[a] The eastern China domain is defined as the area within the red dashed box (20^oN-42^oN,103^oE-123^oE) in Figure 3 of the main text.

[b] NMB: normalized mean bias; R: Pearson correlation coefficient; RMSE: root mean square error

Table S6 Statistical comparisons of the *a priori* and *a posteriori* (from IE-1 and IE-3) simulated glyoxal VCDs against the glyoxal VCDs observed by GOME-2A over eastern China [a]

Month	Glyoxal VCDs (model against GOME-2A observations)								
	NMB [b]			R [b]			RMSE [b] ($\times10^{14}$ molec cm^{-2})		
	a priori	*a posteriori* IE-1	*a posteriori* IE-3	*a priori*	*a posteriori* IE-1	*a posteriori* IE-3	*a priori*	*a posteriori* IE-1	*a posteriori* IE-3
JAN	-0.075	-0.21	-0.14	0.65	0.80	0.61	1.25	0.900	1.23
FEB	-0.15	-0.19	-0.16	0.67	0.76	0.67	0.900	0.723	0.892
MAR	-0.44	-0.33	-0.36	0.67	0.64	0.65	1.59	1.43	1.48
APR	-0.55	-0.44	-0.55	0.85	0.78	0.85	1.67	1.47	1.66
MAY	-0.59	-0.32	-0.39	0.80	0.83	0.79	1.64	1.02	1.18
JUN	-0.55	-0.32	-0.33	0.80	0.85	0.86	2.14	1.52	1.51
JUL	-0.53	-0.31	-0.29	0.89	0.87	0.88	1.90	1.23	1.21
AUG	-0.52	-0.34	-0.33	0.74	0.77	0.75	1.82	1.31	1.30
SEP	-0.56	-0.41	-0.41	0.77	0.73	0.62	1.85	1.47	1.54
OCT	-0.48	-0.33	-0.44	0.85	0.83	0.83	1.44	1.09	1.33
NOV	-0.25	-0.26	-0.40	0.72	0.82	0.77	0.94	0.853	1.10
DEC	0.079	-0.21	-0.15	0.60	0.79	0.69	1.18	0.745	0.876

[a] The eastern China domain is defined as the area within the red dashed box (20^oN-42^oN,103^oE-123^oE) in Figure 3 of the main text.

[b] NMB: normalized mean bias; R: Pearson correlation coefficient; RMSE: root mean square error

Table S7 Statistical comparisons of the *a priori* and *a posteriori* (from IE-2 and IE-4) simulated formaldehyde VCDs against the formaldehyde VCDs observed by OMI over eastern China [a]

Month	Formaldehyde VCDs (model against OMI observations)								
	NMB [b]			R [b]			RMSE [b] ($\times10^{15}$ molec cm^{-2})		
	a priori	*a posteriori* IE-2	*a posteriori* IE-4	*a priori*	*a posteriori* IE-2	*a posteriori* IE-4	*a priori*	*a posteriori* IE-2	*a posteriori* IE-4
JAN	0.38	0.12	0.40	0.85	0.86	0.84	1.94	0.78	2.01
FEB	0.46	0.18	0.49	0.85	0.94	0.83	1.90	0.87	2.04
MAR	0.22	0.081	0.29	0.93	0.97	0.90	1.37	0.72	1.74
APR	0.38	0.22	0.45	0.88	0.93	0.86	1.96	1.24	2.26
MAY	0.47	0.29	0.56	0.94	0.89	0.95	2.56	1.71	3.04
JUN	0.25	0.16	0.39	0.81	0.84	0.81	2.45	1.82	3.39
JUL	0.27	0.19	0.41	0.81	0.84	0.77	2.49	1.96	3.69
AUG	0.38	0.24	0.58	0.85	0.85	0.80	2.82	1.96	4.36
SEP	0.36	0.15	0.48	0.84	0.83	0.82	2.29	1.30	3.10
OCT	0.29	0.10	0.38	0.94	0.94	0.92	1.59	0.85	2.08
NOV	0.36	0.16	0.42	0.84	0.86	0.84	1.78	0.97	2.02
DEC	0.70	0.23	0.72	0.83	0.92	0.83	2.66	1.00	2.75

[a] The eastern China domain is defined as the area within the red dashed box (20^oN-42^oN,103^oE-123^oE) in Figure 3 of the main text.

[b] NMB: normalized mean bias; R: Pearson correlation coefficient; RMSE: root mean square error

Table S8 Statistical comparisons of the *a priori* and *a posteriori* (from IE-2 and IE-4) simulated glyoxal VCDs against the glyoxal VCDs observed by OMI over eastern China [a]

Month	Glyoxal VCDs (model against OMI observations)								
	NMB			R			RMSE ($\times10^{14}$ molec cm^{-2})		
	a priori	*a posteriori* IE-2	*a posteriori* IE-4	*a priori*	*a posteriori* IE-2	*a posteriori* IE-4	*a priori*	*a posteriori* IE-2	*a posteriori* IE-4
JAN	-0.32	-0.33	-0.29	0.12	0.077	0.10	1.40	1.34	1.28
FEB	-0.46	-0.36	-0.32	0.45	0.38	0.33	1.49	1.32	1.26
MAR	-0.60	-0.38	-0.33	0.69	0.39	0.38	2.41	2.00	1.92
APR	-0.63	-0.33	-0.30	0.83	0.46	0.48	2.14	1.63	1.53
MAY	-0.63	-0.58	-0.26	0.82	0.80	0.80	2.04	1.88	1.09
JUN	-0.66	-0.51	-0.29	0.64	0.80	0.88	3.24	2.50	1.60
JUL	-0.65	-0.58	-0.45	0.78	0.79	0.83	2.92	2.63	2.10
AUG	-0.60	-0.50	-0.32	0.68	0.78	0.80	2.35	1.96	1.45
SEP	-0.65	-0.17	-0.16	0.68	0.61	0.75	2.35	1.35	1.05
OCT	-0.61	-0.14	-0.15	0.87	0.90	0.89	1.96	0.733	0.73
NOV	-0.46	-0.34	-0.28	0.53	0.48	0.52	1.39	1.19	1.09
DEC	-0.35	-0.38	-0.30	0.28	0.38	0.37	1.44	1.38	1.28

[a] The eastern China domain is defined as the area within the red dashed box (20^oN-42^oN,103^oE-123^oE) in Figure 3 of the main text.

[b] NMB: normalized mean bias; R: Pearson correlation coefficient; RMSE: root mean square error

Table S9 Comparison of measured and simulated surface ozone concentrations over China

Reference	Location	Platform	Time	Mixing ratio (ppb)			Bias (model - observation)	
				observations	*a priori* emissions [a]	average top-down emissions [a]	*a priori* emissions [a]	average top-down emissions [a]
Wang et al. (2012)	Beijing (39.8°N, 116.47°E)	Ozone sonde	14:00 LT, June 2002-2010	100 to 120	97	103	-23 to -3	-17 to 3
			14:00 LT, December 2002-2010	0 to 30	46	38	16 to 46	8 to 38
Sun et al. (2016)	Mt. Tai (36.25°N, 117.10°E, 1533 m a.s.l.)	Ground-based	Maximum daily 8h-average, June 2006-2015	108	97	103	-11	-5
Li et al. (2007)	Mt. Tai (36.25°N, 117.10°E, 1533 m a.s.l.)	Ground-based	13-17 LT, December 2004	46	46	38	0	-8
Li et al. (2007)	Mt. Hua (110.09°E, 34.49°N, 2064 m a.s.l.)	Ground-based	13-17 LT, June 2004	76	74	78	-2	2
			13-17 LT, December 2004	38	56	51	18	13
Xu et al. (2008)	Lin'an (30°3N, 119°7E, 139 m a.s.l.)	Ground-based	13-17 LT, June 2006	62	57	59	-5	-3
			13-17 LT, December 2005	27	56	48	29	21
Xu et al. (2016)	Waliguan (36.28°N, 100.9°E, 3816 m a.s.l.)	Ground-based	11-16 LT, June 1994-2013	61	60	61	-1	0
			11-16 LT, December 1994-2013	41	47	47	6	6
Zheng	Huizhou	Groun	13-17 LT,	34	36	36	2	2

et al. (2010)	(114.4°E,23.09°N)	d-based	June 2007					
			13-17 LT, December 2007	66	61	59	-5	-7
J.M. Zhang et al. (2009)	Lanzhou (36.13°N, 103.69°E, 1631m a.s.l.)	Ground-based	13-17 LT, June 2006	74	67	68	-7	-6
Li et al. (2015)	Changchun (43.9°N, 125.2°E, 237 m a.s.l.)	Ozone sonde	14 LT, June 13, 2013	62	66	69	4	7
Wang et al. (2015)	Akedala (47.1°N, 87.5°E, 502 m a.s.l.)	Ground-based	13-17 LT, July 2013	53	56	56	3	3
			13-17 LT, November 2013	21	36	36	15	15

[a] Simulated surface ozone concentrations were sampled from 13:00 to 17:00 local time.

Table S10 Surface measurements of SOC concentrations in June during 2006 and 2007 (Zhang et al., 2012)[a] and comparison to simulated SOC concentrations

Site	Site type	SOC concentration (μg C m^{-3})			Bias (model - measurement)	
		measurement	*a priori* simulation	average top-down emission estimates simulation	*a priori* simulation	average top-down emission estimates simulation
Chengdu (30.65°N, 104.03°E)	urban	3.79	1.31	1.61	-2.49	-2.18
Dalian (38.9°N, 121.63°E)	urban	2.64	1.32	2.09	-1.32	-0.55
Dunhuang (40.15°N, 94.68°E)	regional	2.51	0.38	0.41	-2.13	-2.11
Gaolanshan (36.0°N, 105.85°E)	regional	1.29	0.73	0.97	-0.56	-0.32
Jinsha (29.63°N, 114.2°E)	regional	1.81	1.40	1.85	-0.42	0.03
Lhasa (29.67°N, 91.13°E)	regional	2.34	0.47	0.48	-1.88	-1.86
LinAn (30.3°N, 119.73°E)	regional	2.51	0.95	1.29	-1.55	-1.22
Longfengshan (44.73°N, 127.6°E)	regional	1.89	0.85	1.09	-1.04	-0.79
Nanning (22.82°N, 108.35°E)	urban	1.70	0.72	0.74	-0.98	-0.96
Taiyangshan (29.17°N, 111.71°E)	regional	1.11	1.38	1.72	0.27	0.61
XiAn (34.43°N, 108.97°E)	urban	5.41	1.70	2.39	-3.71	-3.02
Zhengzhou (34.78°N, 113.68°E)	urban	2.78	1.59	2.17	-1.19	-0.62

Average		2.48	1.07	1.40	-1.42	-1.08

[a] SOC concentrations were computed using organic carbon measurements (μgC m^{-3}) and the EC-tracer approach (Zhang et al., 2012).

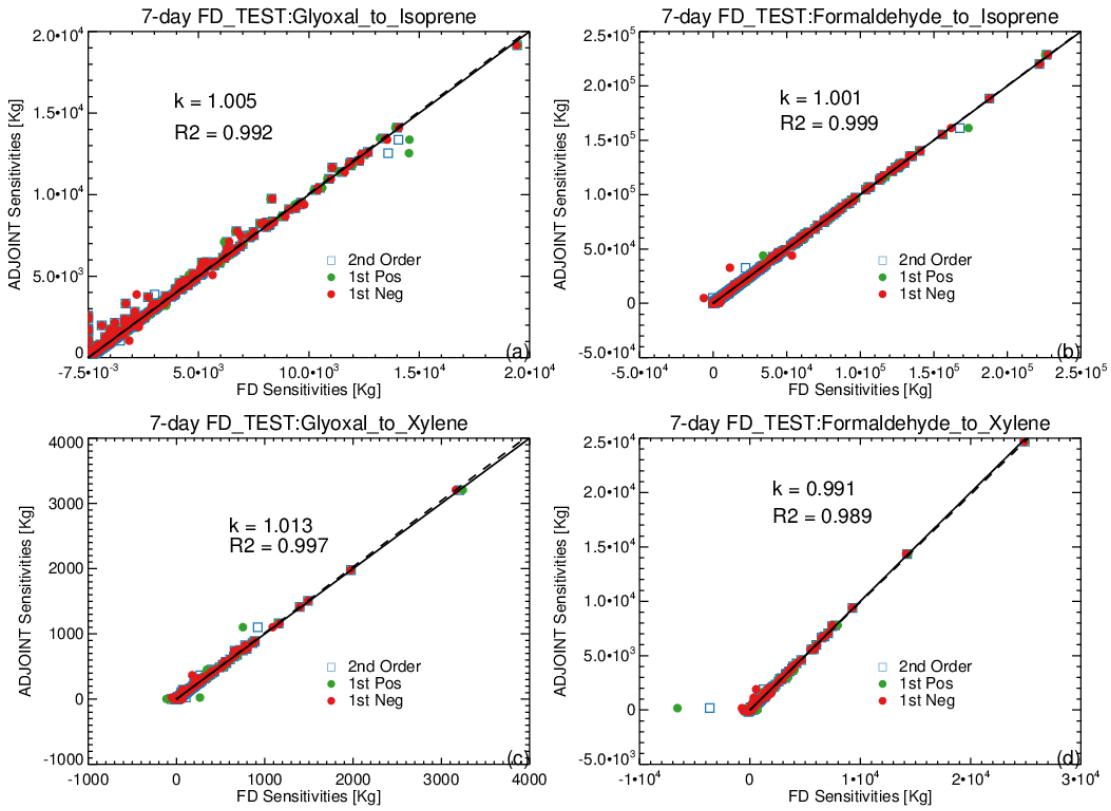

Figure S1. Finite difference test for the GEOS-Chem adjoint model for the period between July 1st and July 7th, 2007. (a): Sensitivities of global glyoxal burden to biogenic isoprene emission scale factor; (b): sensitivities of global formaldehyde burden to biogenic isoprene emission scale factor; (c) sensitivities of global glyoxal burden to anthropogenic xylene emission scale factor; (d): sensitivities of global formaldehyde burden to anthropogenic xylene emission scale factor. ADJOINT sensitivities and FD sensitivities were calculated by the adjoint model and the forward model, respectively. '2nd Order', '1st Pos' and '1st Nes' represent sensitivities calculated by central, forward, backward finite difference methods, respectively. The slopes of the regression lines (k) and the correlations (R^2) are shown in set.

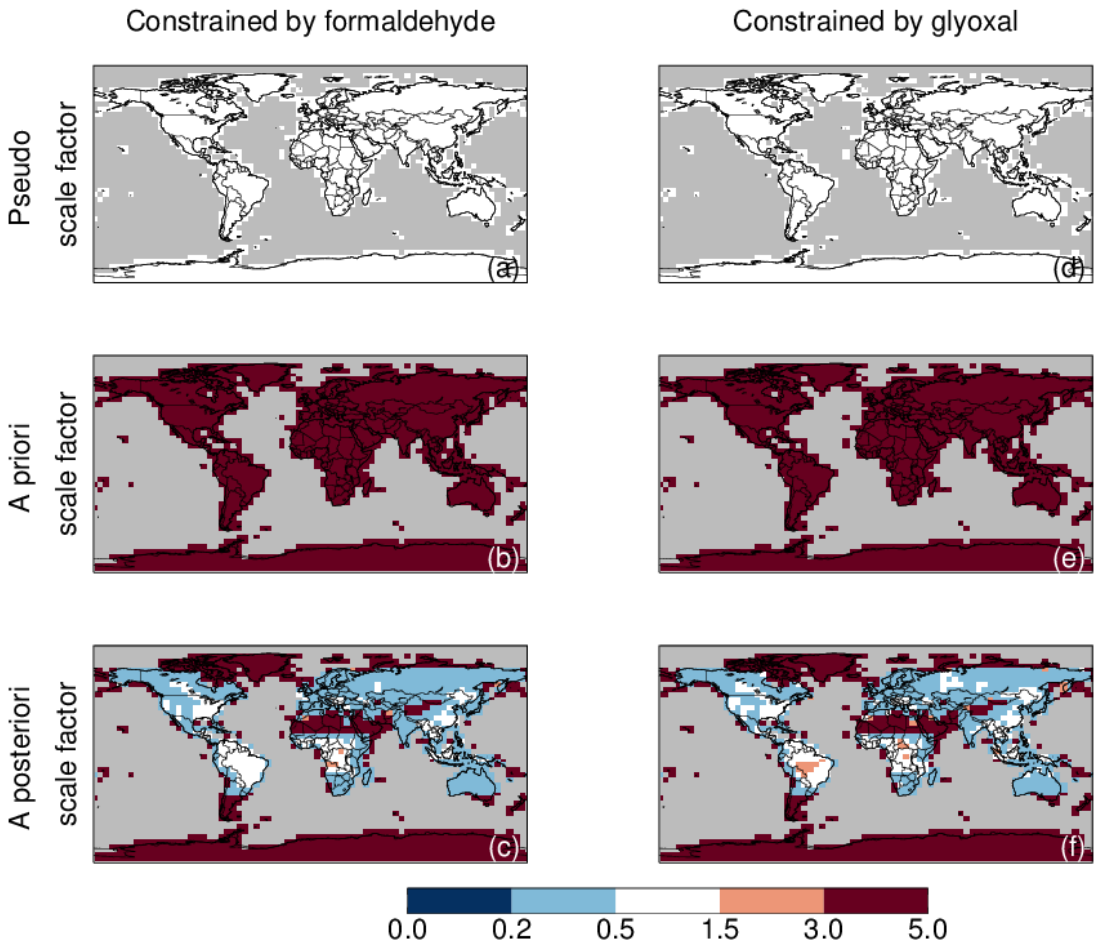

Figure S2. Pseudo isoprene emission scale factor ((a) and (d), uniformly set to 1.0 to generate pseudo observations), the *a priori* isoprene emission scale factor ((b) and (e), uniformly set to 5.0), and the *a posteriori* isoprene emission scale factor ((c) and (f)) in inversion tests (July 1th to 7th, 2007) constrained by pseudo observations of formaldehyde and glyoxal, respectively.

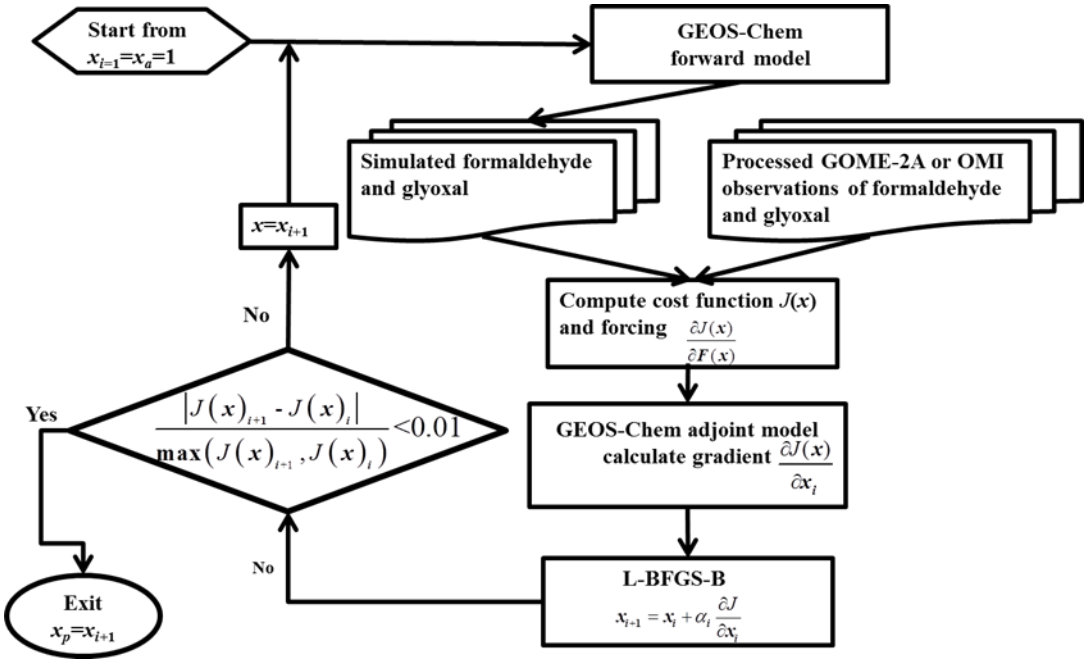

Figure S3. Protocol for the inversion experiments. For each month, we began by driving the GEOS-Chem forward model with the *a priori* emissions ($x_{i=1} = x_a = 1$) to simulate the monthly mean formaldehyde and glyoxal VCDs at satellite-crossing time. The simulated and satellite-observed VCDs were used to calculate the cost function, $J(x)$, and the forcing arrays ($\frac{\partial J(x)}{\partial F(x)}$). The adjoint of GEOS-Chem was then used to compute the cost function gradient ($\frac{\partial J(x)}{\partial x}$), and the next guess of the emission scale factor (x_{i+1}) was calculated using the Quasi-Newton L-BFGS-B algorithm (Byrd et al., 1995; Zhu et al., 1997), subject to the bounds $0.32 \leq x \leq 10$. These bounds were selected based on the largest uncertainties quoted in the literature on Chinese NMVOC emission estimates (Q. Zhang et al., 2009; Liu et al., 2012). The process was then iterated until the incremental relative reduction of the cost function ($\frac{|J(x)_{i+1} - J(x)_i|}{\max(J(x)_{i+1}, J(x)_i)}$) was less than 1% after at least five iterations. We took x_{i+1} from the last iteration as the optimized emission scale factor (x_p) and applied it to calculate the top-down emission estimate.

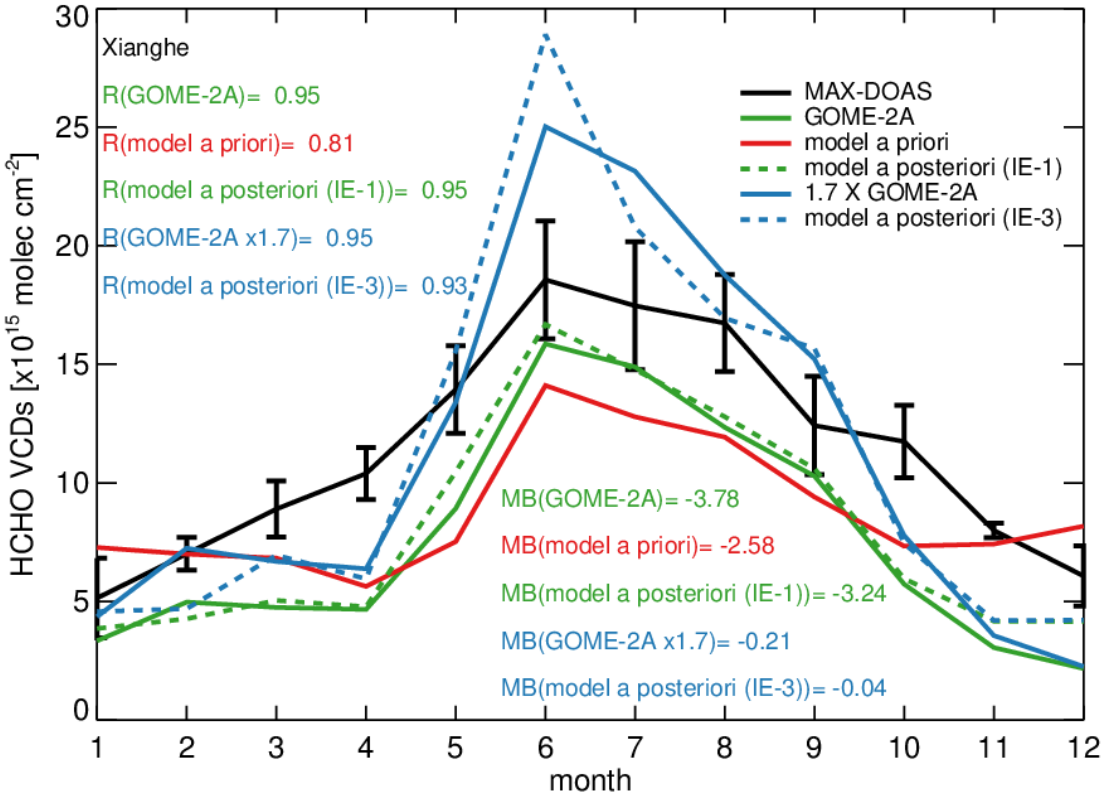

Figure S4. Measured and simulated monthly mean formaldehyde VCDs at Xianghe at GOME-2A overpass time: MAX-DOAS measurements (black line, monthly mean averages for the years 2010 to 2016 from Vlemmix et al., 2015), GOME-2A measurements (green solid line), GOME-2A measurements multiplied by 1.7 (blue solid line), monthly mean formaldehyde VCDs from the *a priori* simulation (red line), the IE-1 *a posteriori* simulation (green dashed line), and the IE-3 *a posteriori* simulation (blue dashed line). Pearson correlation coefficients (R) of the satellite-observed and simulated formaldehyde VCDs against the MAX-DOAS measurements are shown in the top left. Annual mean biases (MB, in units of 10^{15} molecules cm^{-2}) of the satellite-observed and simulated formaldehyde VCDs against the MAX-DOAS measurements are shown in the bottom right.

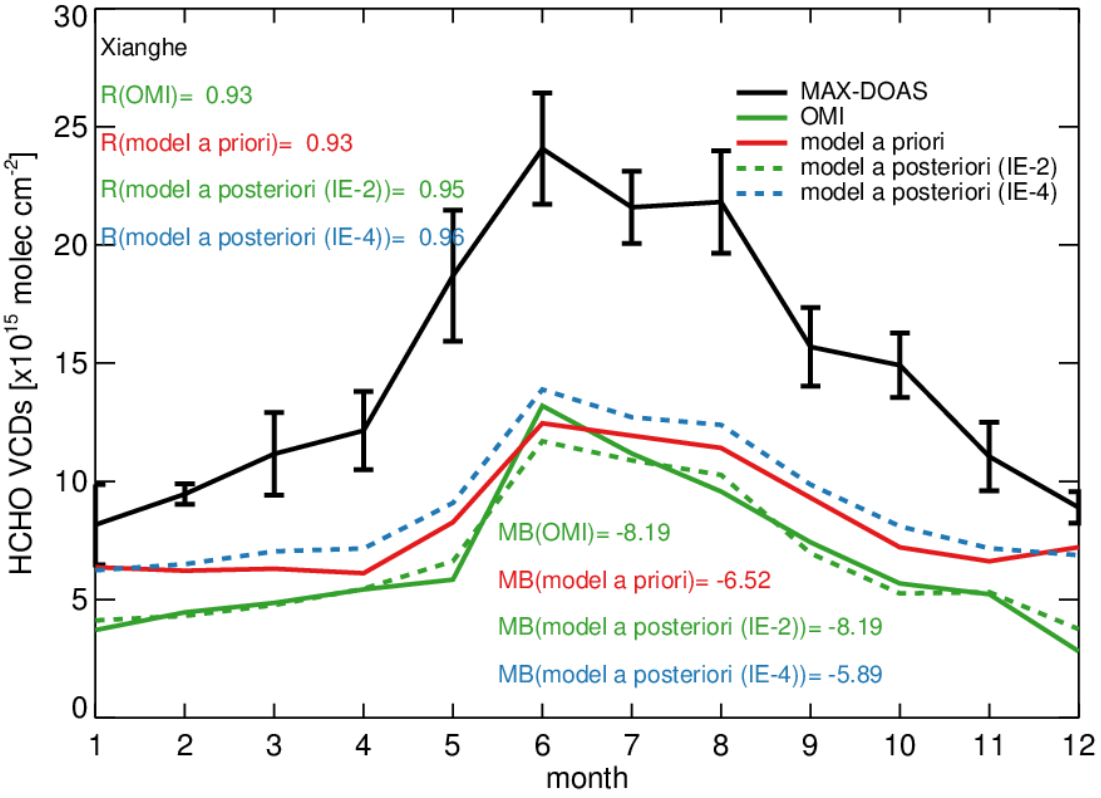

Figure S5 Measured and simulated monthly mean formaldehyde VCDs at Xianghe at OMI overpass time: MAX-DOAS measurements (black line, monthly mean averages for the years 2010 to 2016 from Vlemmix et al., 2015), OMI measurements (green solid line), monthly mean formaldehyde VCDs from the *a priori* simulation (red line), the IE-2 *a posteriori* simulation (green dashed line), and the IE-4 *a posteriori* simulation (blue dashed line). Pearson correlation coefficients (R) of the satellite-observed and simulated formaldehyde VCDs against the MAX-DOAS measurements are shown in the top left. Annual mean biases (MB, in units of 10^{15} molecules cm^{-2}) of the satellite-observed and simulated formaldehyde VCDs against the MAX-DOAS measurements are shown in the bottom right.

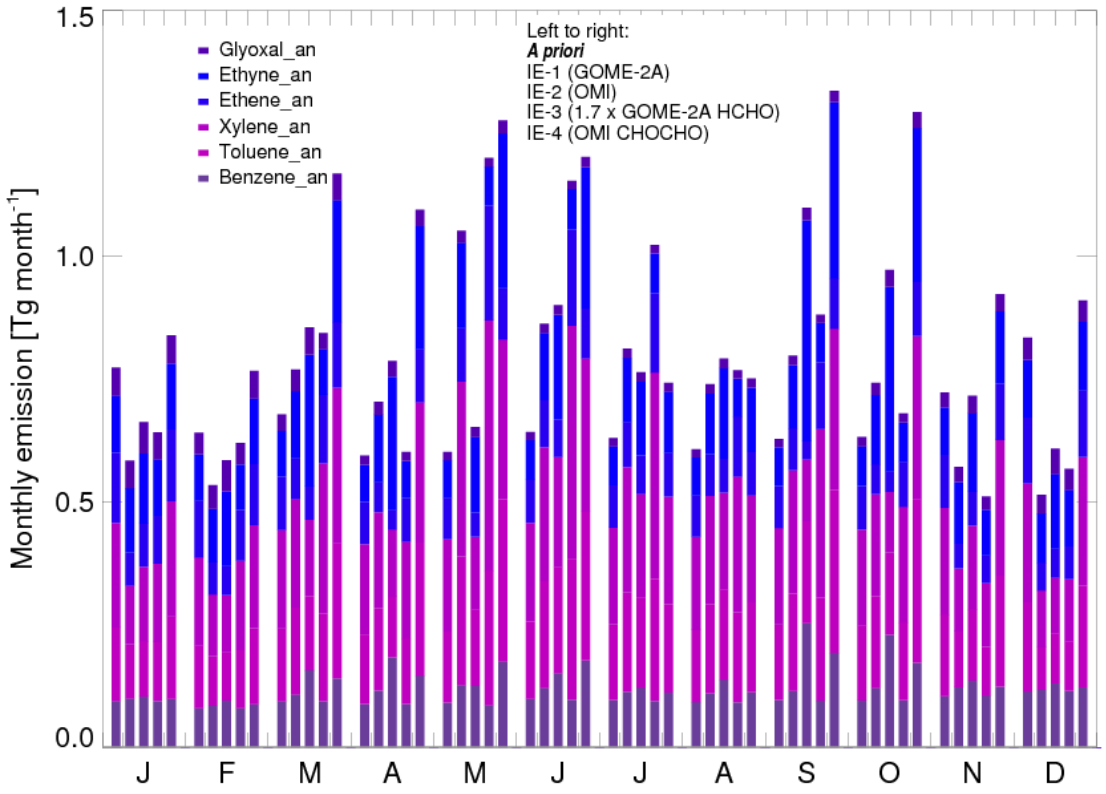

Figure S6. Comparison of the *a priori* and *a posteriori* monthly Chinese anthropogenic glyoxal precursors emission estimates for the year 2007. The bars from left to right for each month represent the *a priori* emission estimates, and the *a posteriori* emission estimates from IE-1, IE-2, IE-3, and IE-4, respectively. Color keys for the NMVOC species are shown inset; the suffix 'an' indicates the anthropogenic source.

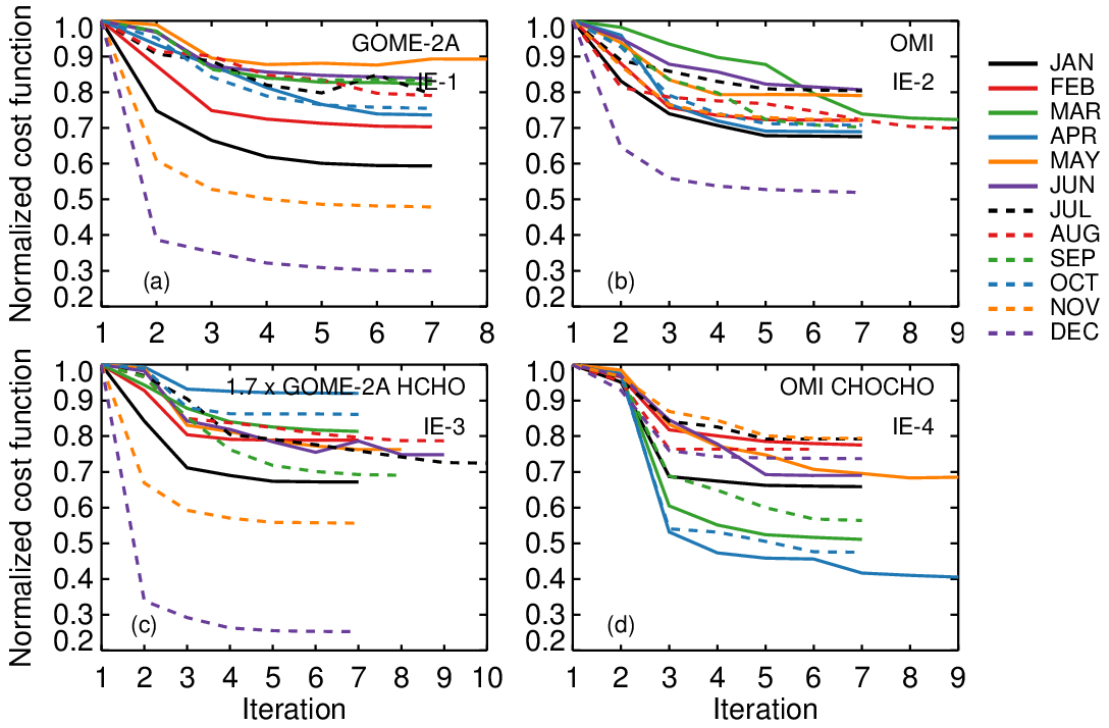

Figure S7. Change in the normalized cost function ($J(x)_i$ / $J(x)_{i=1}$) over China in the four inversion experiments: (a) IE-1, (b) IE-2, (c) IE-3, and (d) IE-4.

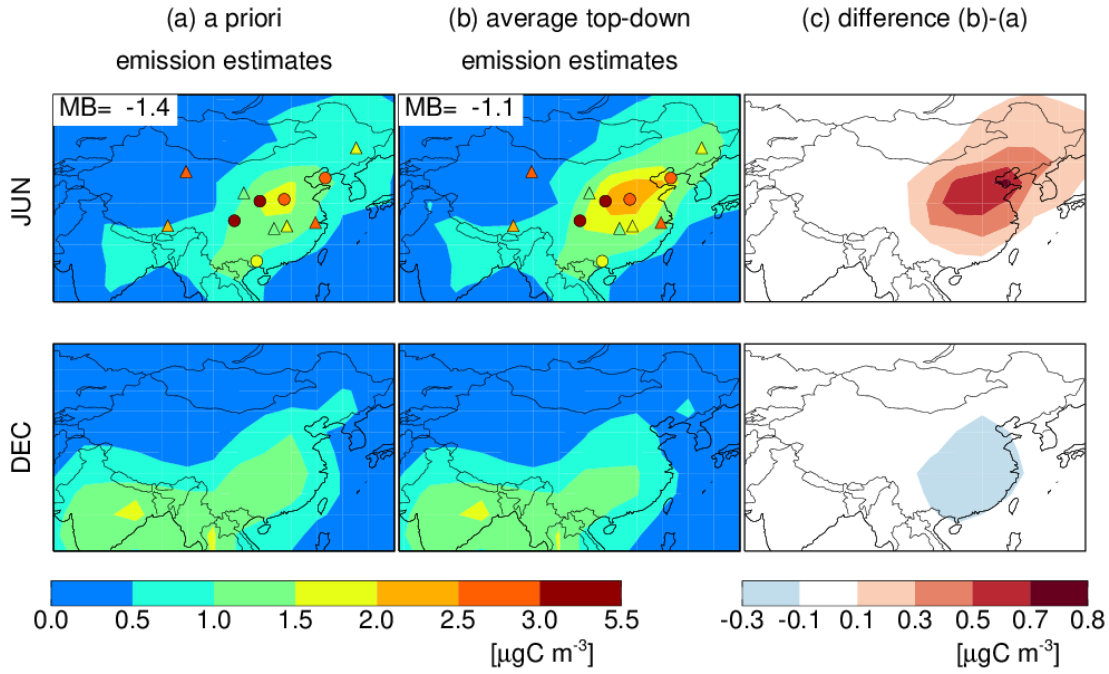

Figure S8. Simulated monthly mean surface secondary organic carbon (SOC) concentrations in June and December 2007 driven by (a) the *a priori* emissions and (b) our average top-down emissions, respectively, as well as (c) the differences. Overlaid symbols show the SOC measurements at 12 urban (circles) and regional (triangles) sites in China in June (Table S10). Mean biases (MB) of the simulated concentrations relative to surface measurements in June are shown inset.

Reference

Acarreta, J. R., De Haan, J. F., and Stammes, P.: Cloud pressure retrieval using the O2-O2absorption band at 477 nm, J. Geophys. Res., 109, doi: 10.1029/2003jd003915, 2004.

Boersma, K. F., Eskes, H. J., and Brinksma, E. J.: Error analysis for tropospheric NO2retrieval from space, Journal of Geophysical Research: Atmospheres, 109, D04311, doi:10.1029/2003jd003962, 2004.

Byrd, R. H., Lu, P. H., Nocedal, J., and Zhu, C. Y.: A Limited Memory Algorithm for Bound Constrained Optimization, Siam J. Sci. Comput., 16, 1190-1208, doi: 10.1137/0916069, 1995.

Chan Miller, C., Gonzalez Abad, G., Wang, H., Liu, X., Kurosu, T., Jacob, D. J., and Chance, K.: Glyoxal retrieval from the Ozone Monitoring Instrument, Atmos. Meas. Tech., 7, 3891-3907, doi:10.5194/amt-7-3891-2014, 2014.

De Smedt, I., Van Roozendael, M., Stavrakou, T., Müller, J. F., Lerot, C., Theys, N., Valks, P., Hao, N., and van der A, R.: Improved retrieval of global tropospheric formaldehyde columns from GOME-2/MetOp-A addressing noise reduction and instrumental degradation issues, Atmos. Meas. Tech., 5, 2933-2949, doi:10.5194/amt-5-2933-2012, 2012.

González Abad, G., Liu, X., Chance, K., Wang, H., Kurosu, T. P., and Suleiman, R.: Updated Smithsonian Astrophysical Observatory Ozone Monitoring Instrument (SAO OMI) formaldehyde retrieval, Atmos. Meas. Tech., 8, 19-32, doi:10.5194/amt-8-19-2015, 2015.

Kleipool, Q. L., Dobber, M. R., de Haan, J. F., and Levelt, P. F.: Earth surface reflectance climatology from 3 years of OMI data, Journal of Geophysical Research, 113, doi: 10.1029/2008jd010290, 2008.

Kleipool, Q. L.: Transient signal flagging algorithm definition for radiance data, Tech. Rep. TN-OMIE-KNMI-717 TN-OMIEKNMI-717 TN-OMIE-KNMI-717 TN-OMIE-KNMI-717 TNOMIE-KNMI-717, Royal Netherlands Meteorological Institute, De Bilt, the Netherlands, 2005.

Lee, H., Ryu, J., Irie, H., Jang, S.-H., Park, J., Choi, W., and Hong, H.: Investigations of the Diurnal Variation of Vertical HCHO Profiles Based on MAX-DOAS Measurements in Beijing: Comparisons with OMI Vertical Column Data, Atmosphere, 6, 1816-1832, doi: 10.3390/atmos6111816, 2015.

Lerot, C., Stavrakou, T., De Smedt, I., Muller, J. F., and Van Roozendael, M.: Glyoxal vertical columns from GOME-2 backscattered light measurements and comparisons with a global model, Atmos. Chem. Phys., 10, 12059-12072, doi: 10.5194/acp-10-12059-2010, 2010.

Li, D., and Bian, J. C.: Observation of a Summer Tropopause Fold by Ozonesonde at Changchun, China: Comparison with Reanalysis and Model Simulation, Adv. Atmos. Sci., 32, 1354-1364, doi: 10.1007/s00376-015-5022-x, 2015.

Li, J., Wang, Z. F., Akimoto, H., Gao, C., Pochanart, P., and Wang, X. Q.: Modeling study of ozone

seasonal cycle in lower troposphere over east Asia, J. Geophys. Res. Atmos., 112, doi: 10.1029/2006JD008209, 2007.

Li, X., Brauers, T., Hofzumahaus, A., Lu, K., Li, Y. P., Shao, M., Wagner, T., and Wahner, A.: MAX-DOAS measurements of NO2, HCHO and CHOCHO at a rural site in Southern China, Atmos. Chem. Phys., 13, 2133-2151, doi: 10.5194/acp-13-2133-2013, 2013.

Liu, Z., Wang, Y., Vrekoussis, M., Richter, A., Wittrock, F., Burrows, J. P., Shao, M., Chang, C.-C., Liu, S.-C., Wang, H., and Chen, C.: Exploring the missing source of glyoxal (CHOCHO) over China, Geophys. Res. Lett., 39, doi:10.1029/2012gl051645, 2012.

Spurr, R.: LIDORT and VLIDORT: Linearized pseudo-spherical scalar and vector discrete ordinate radiative transfer models for use in remote sensing retrieval problems, in: Light Scattering Reviews, edited by: Kokhanovsky, A., Springer, 3, 229–275, 2008.

Spurr, R. J. D.: VLIDORT: A linearized pseudo-spherical vector discrete ordinate radiative transfer code for forward model and retrieval studies in multilayer multiple scattering media, J. Quant. Spectrosc. Radiat. Transf., 102, 316-342, doi: 10.1016/j.jqsrt.2006.05.005, 2006.

Stavrakou, T., Muller, J. F., De Smedt, I., Van Roozendael, M., van der Werf, G. R., Giglio, L., and Guenther, A.: Global emissions of non-methane hydrocarbons deduced from SCIAMACHY formaldehyde columns through 2003-2006, Atmos. Chem. Phys., 9, 3663-3679, doi:10.5194/acp-9-3663-2009, 2009b.

Sun, L., Xue, L. K., Wang, T., Gao, J., Ding, A. J., Cooper, O. R., Lin, M. Y., Xu, P. J., Wang, Z., Wang, X. F., Wen, L., Zhu, Y. H., Chen, T. S., Yang, L. X., Wang, Y., Chen, J. M., and Wang, W. X.: Significant increase of summertime ozone at Mount Tai in Central Eastern China, Atmos. Chem. Phys., 16, 10637-10650, doi: 10.5194/acp-16-10637-2016, 2016.

Vlemmix, T., Hendrick, F., Pinardi, G., Smedt, I., De Fayt, C., Hermans, C., Piters, A., Wang, P., and Levelt, P.: MAX-DOAS observations of aerosols, formaldehyde and nitrogen dioxide in the Beijing area: comparison of two profile retrieval, Atmos. Meas. Tech., 2, 941–963, doi:10.5194/amt-8-941-2015, 2015.

Wang, H. Q., Ma, J. M., Shen, Y. J., and Wang, Y. A.: Assessment of Ozone Variations and Meteorological Influences at a Rural Site in Northern Xinjiang, Bull. Environ. Contam. Tox., 94, 240-246, doi: 10.1007/s00128-014-1451-y, 2015.

Wang, Y., Beirle, S., Lampel, J., Koukouli, M., De Smedt, I., Theys, N., Li, A., Wu, D. X., Xie, P. H., Liu, C., Van Roozendael, M., Stavrakou, T., Muller, J. F., and Wagner, T.: Validation of OMI, GOME-2A and GOME-2B tropospheric NO2, SO2 and HCHO products using MAX-DOAS observations from 2011 to 2014 in Wuxi, China: investigation of the effects of priori profiles and aerosols on the satellite products, Atmos. Chem. Phys., 17, 5007-5033, doi: 10.5194/acp-17-5007-2017, 2017.

Wang, P., Stammes, P., R., v. d. A., Pinardi, G., and Roozendael, M. V.: FRESCO+: an improved O2 A-band cloud retrieval algorithm for tropospheric trace gas retrievals, Atmos. Chem. Phys., 8, 6565-6576, doi: 10.5194/acp-8-6565-2008, 2008.

Wang, Y., Konopka, P., Liu, Y., Chen, H., Muller, R., Ploger, F., Riese, M., Cai, Z., and Lu, D.: Tropospheric ozone trend over Beijing from 2002-2010: ozonesonde measurements and modeling analysis, Atmos. Chem. Phys., 12, 8389-8399, doi: 10.5194/acp-12-8389-2012, 2012.

Xu, W. Y., Lin, W. L., Xu, X. B., Tang, J., Huang, J. Q., Wu, H., and Zhang, X. C.: Long-term trends of surface ozone and its influencing factors at the Mt Waliguan GAW station, China - Part 1: Overall trends and characteristics, Atmos. Chem. and Phys., 16, 6191-6205, doi: 10.5194/acp-16-6191-2016, 2016.

Xu, X., Lin, W., Wang, T., Yan, P., Tang, J., Meng, Z., and Wang, Y.: Long-term trend of surface ozone at a regional background station in eastern China 1991-2006: enhanced variability, Atmos. Chem. Phys., 8, 2595-2607, doi: 10.5194/acp-8-2595-2008, 2008.

Zhang, J. M., Wang, T., Ding, A. J., Zhou, X. H., Xue, L. K., Poon, C. N., Wu, W. S., Gao, J., Zuo, H. C., Chen, J. M., Zhang, X. C., and Fan, S. J.: Continuous measurement of peroxyacetyl nitrate (PAN) in suburban and remote areas of western China, Atmos. Environ., 43, 228-237, doi: 10.1016/j.atmosenv.2008.09.070, 2009.

Zhang, Q., Streets, D. G., Carmichael, G. R., He, K. B., Huo, H., Kannari, A., Klimont, Z., Park, I. S., Reddy, S., Fu, J. S., Chen, D., Duan, L., Lei, Y., Wang, L. T., and Yao, Z. L.: Asian emissions in 2006 for the NASA INTEX-B mission, Atmos. Chem. Phys., 9, 5131-5153, 10.5194/acp-9-5131-2009, 2009.

Zhang, X. Y., Wang, Y. Q., Niu, T., Zhang, X. C., Gong, S. L., Zhang, Y. M., and Sun, J. Y.: Atmospheric aerosol compositions in China: spatial/temporal variability, chemical signature, regional haze distribution and comparisons with global aerosols, Atmospheric Chemistry and Physics, 12, 779-799, doi:10.5194/acp-12-779-2012, 2012.

Zheng, J. Y., Zhong, L. J., Wang, T., Louie, P. K. K., and Li, Z. C.: Ground-level ozone in the Pearl River Delta region: Analysis of data from a recently established regional air quality monitoring network, Atmos. Environ., 44, 814-823, doi: 10.1016/j.atmosenv.2009.11.032, 2010.

Zhu, C. Y., Byrd, R. H., Lu, P. H., and Nocedal, J.: Algorithm 778: L-BFGS-B: Fortran subroutines for large-scale bound-constrained optimization, ACM T. Math. Software, 23, 550-560, doi: 10.1145/279232.279236, 1997.